DOI: 10.26599/FSHW.2024.9250062

Contents lists available at SciOpen

Food Science and Human Wellness

journal homepage: https://www.sciopen.com/journal/2097-0765

Unraveling the trans-epithelial absorption of novel dark blue pigment from *Vaccinium bracteatum* Thunb. leaves on the Caco-2 intestinal cell

Mingcong Fan[a], Weijia Lian[a], Wenjun Yao[a], Tingting Li[b], Jiajia Zhao[c], Qiang Li[d], Yanming Guan[e], Yan Li[a], Haifeng Qian[a], Zhiming Rao[f], Li Wang[a,*]

[a] *School of Food Science and Technology, State Key Laboratory of Food Science and Technology, National Engineering Research Center for Functional Food, Jiangnan University, Wuxi 214122, China*

[b] *Department of Food Science and Engineering, College of Light Industry and Food Engineering, Nanjing Forestry University, Nanjing 210037, China*

[c] *College of Cooking Science and Technology, Jiangsu College of Tourism, Yangzhou 225000, China*

[d] *China National Institute of Standardization, Beijing 100089, China*

[e] *China National Research Institute of Food and Fermentation Industries Co. Ltd, Beijing 100015, China*

[f] *School of Biotechnology, Jiangnan University, Wuxi 214122, China*

ABSTRACT: The dark blue pigment (DBP) is a health ingredient from *Vaccinium bracteatum* Thunb. leaves used as a functional food supplement. However, the details of transepithelial absorption on the intestinal epithelial cells are barely understood. This study aimed to clarify the absorption properties of DBP in the Caco-2 cell monolayer model and evaluate the effect on the endo-metabolism and barrier function of Caco-2 cells. The results showed that the DBP did not show the dose-dependent toxic effect to Caco-2 cells between 0.25 and 1.5 mg/mL, which did not cause disorder in the normal cell metabolism and absorption activity. The Caco-2 cells monolayer model could absorb DBP by passive and active transport, and the absorptive pattern was dose-dependent when the concentration was more than 0.25 mg/mL. During DBP absorption, an increase in mRNA and protein expressions of glucose transporters demonstrated that the glucose transporters were the potential transporter of DBP. But the glucose transport amounts were significantly lowered after 30 min of DBP treatment, indicating that DBP owned the inhibitory effect on glucose transportation. Furthermore, DBP also owned protective effects on the barrier function of intestinal epithelial cells.

Keywords: *Vaccinium bracteatum* Thunb. Leaf; Dark blue pigment (DBP), Intestinal epithelial cell; Transepithelial absorption; Epithelial cell barrier

1. Introduction

Vaccinium bracteatum Thunb. is an evergreen shrubby herb growing in the mountainous areas in East and Southeast Asia. *V. bracteatum* Thunb. leaves (VBTL) can be used as a food colorant, food preservative, and valuable Chinese medicine to heal inflammation, skin eruptions, and other ailments[1]. The identified individual compounds in VBTL to date are more than 150, such as flavonoids, triterpenes, iridoids, and phenylpropanoids[2-4]. Many important pharmacological properties *in vitro* and *in vivo*, including hypoglycemic effect, antioxidant and antimicrobial effect, anti-inflammatory effect, and antidepressant effect

***Corresponding author**
wl0519@163.com (L. Wang)

Received 26 April 2023
Received in revised from 14 June 2023
Accepted 2 August 2023

have been confirmed to be related to these phytochemicals[5-9]. In addition to being a traditional Chinese medicine, the popular primary use of VBTL is consumed as the colorant to dye and cook the traditional rice product “Wu mi Fan”. This dyed rice product with characteristic dark blue color has been recorded in the “Compendium of Materia Medica” as a functional food with the effects of invigorating the body, maintaining agerasia, and improving eyesight. Recently, it has been reported that the “Wu mi Fan” can suppress the drastic symptom of the glycemic response of diabetes patients after consuming “Wu mi Fan” as compared with common rice[10].

Regarding the characteristic dark blue color on the surface of “Wu mi”, our research team found that the compounds of dark blue pigment (DBP) are produced from the reaction between the iridoid glycosides of VBTL and the $–NH_2$ residues in rice protein[11]. The iridoid-derived colored compound was detected as an alternating copolymer structure composed of 5*H*-2-pyrindine and its derivatives[12]. After the occurrence of blue color on the '*Wu mi*' grain surface, this DBP was extremely difficult to isolate and purify, and this issue hampered the determination of the structural analysis. Therefore, our research team proposed a simulated preparation method for this DBP based on the two precursors: free iridoids and amino acids[13]. Further, the DBP inhibited pancreatic α-amylase and α-glucosidase, which could support the digestion resistibility of “Wu mi” and showed the potential benefits for the consumption for diabetes patients[14]. It should be noted that the resulting biological activities of nutrients are usually exerted after digestion and absorption. Despite the latest pursuit to investigate some biological properties *in vitro* of this novel DBP from VBTL, it remains a mystery while absorbed in the intestinal tract of the human body.

The intestinal epithelial cells form a physical barrier between the luminal environment and the body, which plays an essential role in maintaining a certain permeability and tightness of the intestinal tract [15-16]. Transportation of nutrients across membranes in the small intestine can occur by one or more of the following modes: carrier-mediated transport, transcytosis, and passive transport via transcellular or paracellular diffusion [17]. However, the absorption of food components with different polarities was quantitatively regulated or interfered with by the natural intestinal transporters to maintain a different apparent permeability coefficient[18]. Most digested nutrients are carried out through hexose transporters, ATP binding cassette transporters, or monocarboxylate transporters[19]. Taking the absorption of common anthocyanins as an example, due to the same chemical structure with the iridoid-derived compounds, some researches showed that several hexose transporters played an essential role in regulating their transportation. When the monolayer model of Caco-2 epithelial cells was treated with anthocyanins for 4 days, the Caco-2 monolayers exhibited higher expression of glucose/fructose transporters (GLUT2) and an increasing transport rate of anthocyanins[20-21]. The common small molecular polyphenols, such as catechins and their derivatives, are believed to be transported by the multi-drug resistance protein 2 (MRP2) and *P*-glycoprotein (MDR1/*P*-gp)[22]. It is worth noting that the compound conformation and molecular size also determine their absorption through the intestinal epithelial cells[23]. For an example of the hexose transporters, the study on the

absorption of anthocyanins with glucoside, di-glucoside, and coumaroyl glucoside moieties indicated that the carboxyl group at C6 position of the glucose tends to be recognized by GLUT2 and GLUT5 transporters[24].

Prior to our series of studies, no other reports have introduced the membrane transport *in vitro* on the DBP derived from iridoid glycosides, whether the commercialized Gardenia blue pigment or the DBP as a potential pigment source applied in human food. Considering this, the aim of this study was to find novel data on the transepithelial absorption efficiency of DBP using the intestinal Caco-2 cells monolayer model. To this end, the absorption model of DBP was proposed, and the influence of DBP on the endo-metabolism of Caco-2 cells was evaluated by performing a quantitative analysis of secondary metabolites. In addition, we also investigated original indications on the expression profiles of the relevant transporters and tight junction proteins (TJs) of the Caco-2 cell at the transcriptional level. The results of this study aim to raise interest in the use of DBP as a natural source of nutritional pigments, thereby paving the way for the development of innovative products based on VBTL.

2. Materials and methods

2.1 Chemicals and reagents

Six years old *Vaccinium bracteatum* Thunb. trees were cultivated in Liyang City, Jiangsu, China (N 31.40925°, E 119.39502°). *Vaccinium bracteatum* Thunb. leaves (VBTL) in the crown layer were randomly handpicked from four separate plots in April 2021. The picked leaves were rapidly cooled with liquid nitrogen and then stored at −80 ℃ until use. The Sephadex G-25 and the solution of Hanks and D'Hanks were purchased from the Yuanye Bio-Technology Co., Ltd (Shanghai, China). The MTT was purchased from Sigma-Aldrich (St. Louis, USA). The β-glucosidase (100 U/mg) was purchased from J&K Scientific Ltd. (Shanghai, China). The trizol reagent was purchased from Thermo Fisher Scientific (CA, USA). The prime script RT system was purchased from Takara Bio Inc. (Kyoto, Japan). All other chemicals used in this study were of analytical grade and provided by Sinopharm Chemical Reagent Co. Ltd. (Shanghai, China).

2.2 Preparation of VBTL dark blue pigments

The fresh VBTL (20.0 g) was pulped with deionized water (100.0 g) for 10 min to obtain VBTL water extract. The water extract was filtered with 4 layers of gauze and then centrifuged at 4 ℃ (10 000 r/min, 15 min) to obtain supernatant. The supernatant was freeze-dried to obtain the crude VBTL extract's dry powder, then re-dissolved in water and hydrolyzed by β-glucosidase for (1−2) h at 37 ℃. The concentrations of VBTL extract powder and β-glucosidase were 2 mg/mL and 8 μg/mL, respectively. After hydrolyzing, the hydrolysis solution was mixed with glycine according to the percentage of 0.1% (*m*/*V*) for 3 h at 50 ℃. The solution turned blue after the color reaction. Then, the blue solution was vacuum-concentrated and freeze-dried to obtain the crude DBP powder. The crude DBP passed through a Sephadex G-15 column (25 cm × 4.0 cm, MW fractionation range: 200−1 500) to prepare the purified DBP, which was first washed with two beds volume of deionized water. The DBP solution was loaded into the column and eluted with water. Each eluting fraction (one-bed volume per fraction) was collected and measured at 585 nm. The eluting fractions with the absorption peak at 585 nm were combined as the purified DBP solution. Then, the solutions were performed

into a chromatographic column (50 mm × 4.0 mm) with XDA-1 amilan resins. The column was washed with the step gradient elution of methanol-water solution. The eluting fractions with the absorption peak at 585 nm were combined as the purified DBP solution. Further, the solution was purified by the Waters preparative HPLC system equipped with a C18 column (Waters XBridge OBD, 19mm × 150 mm, 2.5 μm). Regarding structural determination, nuclear magnetic resonance (NMR) spectrometer (Avance III 400 mHZ, Bruker, Madison, WI) was used to generate the ^{1}H NMR and ^{13}C NMR data of the DBP key compound, with methanol-d_4 as the solvent of NMR (Table S1). The tentative 2D structure of the key compound was drawn by ChemBioDraw Ultra 14.0 (Fig. S1).

2.3 Cell culture

The Caco-2 human intestinal cells were obtained from the Chinese Academy of Sciences (Shanghai, China). The Caco-2 cell culture medium was Dulbecco's modified Eagle's medium (DMEM, Hyclone) supplemented with 15% fetal bovine serum (Gibco) and 1% penicillin-streptomycin (Gibco). The Caco-2 cells were incubated in a CO_2 incubator (Thermo Fisher Scientific Co.) containing 5% at 37 ℃. The fresh media was renewed every 2 days, and the cells used in this study were at passage 40−50. For the MTT assay, Caco-2 cells were seeded into a 96-well plate at a density of 8×10^4 cells/well. After adherent growing, Caco-2 cells were incubated for 24 h under the DBP treatment with different concentrations. At the end of treatment, cells were incubated with MTT for 4 h at 37 ℃. Then, the medium was removed, and 150 μL DMSO was added. The plates were then tested at 570 nm using a BioTek Epoch 2 microplate spectrophotometer (BioTek Instruments Inc., Winooski, VT, USA). The oxidative-damaged model of Caco-2 cell in vitro was established by H_2O_2 treatment with the final concentration of 500 μmol/L for 4 h as the induction condition.

2.4 Metabolite extraction of Caco-2 cells

Briefly, Caco-2 cells (4×10^5 cells) were seeded in the cell culture dish with Φ6 cm and incubated without treatment. After 24 h of cell attachment, the cells were incubated with DBP (0 mg/mL and 0.5 mg/mL) and collected after 12 h. After the treatment, the cell culture medium was removed, and trypsin was added to the culture dishes. Then the cells were resuspended by gentle blowing and washed three times with PBS. The 80% methanol (1.0 mL) was added as a quencher to slow or halt many metabolic processes and aid in the precipitation of cellular proteins. The solutions were turbo-shocked for 30 s and then repeatedly freeze-thawed three times in liquid nitrogen, sonicated at low temperature for 10 min. After placing at −20 ℃ for 1 h, these solutions were centrifuged at 12 000 r/min for 15 min at 4℃, then freeze-dried. The samples were re-dissolved in 600 μL of 50% aqueous acetonitrile and centrifuged at 4 ℃ for 15 min at 12 000 r/min. Afterward, the supernatant was collected for measurement.

2.5 UPLC-QToF-MS analysis

The UPLC-QToF-MS analysis was performed using a Shimadzu ultra-performance liquid chromatography system (LC30AD, Shimadzu Corporation, Japan) coupled with a QToF mass spectrometer (AB Sciex). The system utilized a UPLC BEH amide column (100 m × 2.1 mm, 1.7 μm, Waters). The mobile

phase was 10 mmol/L NH_4FA of 0.1% formic acid solution (A) and acetonitrile (B) in gradient elution mode at a flow rate of 0.3 mL/min. The sample injection volume was set at 2.5 μL. Positive ion (+ve) mode was used under the following optimized conditions: capillary voltage of 3.5 kV; cone voltage of 20 V; source temperature of 100 ℃; desolvation temperature of 400 ℃; collision gas (argon); desolvation gas (nitrogen) with a flow rate of 700 L/h. Data were recorded between *m*/*z* 50 and 1 500 Da with a scan duration of 0.2 s. AB Sciex software was used for all data acquisition and processing, such as peak alignment, peak extraction, and compound identification.

2.6 Transport verification of VBTL dark blue pigment by Caco-2 cells

Caco-2 cells were seeded into 12 inserts with permeable polycarbonate membrane in a 24-well plate (6.5 mm, 3.0 μm pore size, Corning Inc., NY, USA) at a density of 1×10^5 cells/well. Caco-2 cells were cultured for 3 weeks to reach confluence and differentiation. Medium in the culture plates was replaced every 2 days for the first week and every day for the remaining period. The integrity of the Caco-2 cell monolayer was evaluated by measuring the transepithelial electrical resistance (TEER) with a Millicell MERS-2 epithelial voltohmmeter (Millipore, Bedford, MA, USA). Only monolayer cells with a TEER of above 800 Ω/cm^2 could be used for the transport assays.

Before the transport experiments, the pre-warmed HBSS medium (pH 7.4) was used to wash the Caco-2 monolayer cell twice. For the measurement of the apical side (AP) to basolateral side (BL) transport, 0.4 mL of serum-free medium (pH 7.4) with DBP (0.25~1 mg/mL) was added to the AP side, and 0.6 mL of serum-free medium (pH 7.4) without DBP was added to the BL side. During the transport experiments, the monolayer cells were incubated at 37℃, and the solutions were collected from the BL side at a specific time and replaced by the same volume of pre-warmed serum-free medium. For subsequent transport amount analysis, the standard fitting curve of the concentration from 62.5 μg/mL to 1 mg/mL of DBP standard solution showed higher linear relationship (y = 0.748 9x + 0.0496, R^2 = 0.999 4). The transport amounts and transport efficiency of DBP were calculated by equations 1 and 2:

$$Q_n = \sum_{n=1}^{n-1}(C_n \times V_{BL}) \quad \text{Eq. 1}$$

$$Q\% = \frac{Q_n}{C_0 \times V_{AL}} \quad \text{Eq. 2}$$

where Q_n is the amount of DBP on the BL side at each time point; n is the sampling time; C_0 is the initial concentration on each AL side before the transport experiment; C_n is the detected concentration at the n test time point; V_{AL} and V_{BL} are the solution volumes of AL and BL side.

Apparent permeability coefficients (P_{app}) and efflux ratio (R) of DBP were calculated by equations 3 and 4:

$$P_{app} = \frac{(dQ/dt)}{(A \times C_0)} \quad \text{Eq. 3}$$

$$R = P_{app\ (AP\ to\ BL)} / P_{app\ (BL\ to\ AP)} \quad \text{Eq. 4}$$

Where dQ/dt is the amount of DBP transported across the membrane per unit of time; A is the surface area for the cell monolayer membrane; C_0 is the initial concentration on each AL side before the transport experiment; R is the ratio of the absorptive permeability and the secretory permeability.

2.7 Glucose transport of Caco-2 cells under VBTL dark blue pigment treatment

The glucose transport amount was performed as previously reported with some modification[25]. The pre-warmed HBSS medium (pH 7.4) was used to wash the Caco-2 monolayer cell twice. For the measurement of the apical side (AP) to basolateral side (BL) transport, 0.4 mL of DMEM high glucose medium with DBP (0~0.5 mg/mL) was added to the AP side, and 0.6 mL of pre-warmed PBS was added to the BL side. Then, the monolayer cells were incubated at 37 ℃, and the solutions were collected from the BL side at a specific time and replaced by the same volume of pre-warmed PBS. The glucose concentrations in the BL side were detected using a GOD-POD assay kit (Megazyme, K-GLUC).

2.8 Quantitative real-time PCR analysis

The differentiated Caco-2 cells were treated for 12 h with a medium containing DBP at different concentrations (0−0.5 mg/mL). Total RNA in all Caco-2 cell samples was extracted by Trizol reagent (Invitrogen), and the RNA was transcribed into cDNA by the Prime Script RT system (Takara). For real-time PCR, the expression of GAPDH was used as an internal control. The Real-Time PCR System determined the expression levels of GLUT2, GLUT5, MDR1, MRP2, Occludin, Claudin-1, and ZO-1 (StepOnePlus, Applied Biosystems, USA). All primers were designed, and the sequences were listed in Table S2.

2.9 Western blotting analysis

Briefly, RIPA lysis buffer (Beyotime, Shanghai, China) was used to separate proteins from the differently treated samples of Caco-2 cells. The protein concentration was measured with a BCA protein detection reagent (Beyotime, Shanghai, China). An equal volume of protein sample was loaded on a 10% SDS-PAGE and applied to a polyvinylidene fluoride (PVDF) membrane. The membrane was incubated with a specific primary antibody and an enzyme-labeled secondary antibody. The antibodies of GLUT2 (20436-1-AP, 1:1 000), GLUT5 (27571-1-AP, 1:1 000), and GAPDH (10494-1-AP, 1: 5 000) were purchased from ProteinTech Group, and the antibodies of MRP2 (# 12559S, 1:1 000), MDR1 (# 13342S, 1:1 000) were purchased from Cell Signaling Technology. Secondary antibody was purchased from Jackson ImmunoResearch (HRP Goat Anti-Rabbit/Mouse, 1:1 000).

2.10 Statistical analysis

The orthogonal partial least squares discriminant analysis (OPLS-DA) was performed to visualize the control group and treatment group variables based on the SIMCA P+14.1 (Umertrics, Umea, Sweden) according to a previous method[26]. Heatmap and pathway analysis were performed with MetaboAnalyst 5.0 (http://www.metaboanalyst.ca). The pathway analysis algorithms were set as a hypergeometric test for over-representation analysis and relative-betweenness centrality for pathway topology analysis. All experiments were repeated at least 3 times, and data are presented as the mean ± standard deviation (SD). One-way analysis of variance (ANOVA) was performed by SPSS 22.0 (SPSS Inc., Chicago, USA) to assess whether there is a significant difference between the means of two groups ($P < 0.05$).

3. Results and discussion

3.1 Cytotoxicity analysis of dark blue pigment on Caco-2 cell

The results of our previous study showed that more than 65% of DBP from VBTL could enter the intestine after simulated *in vitro* gastrointestinal digestion, where the DBP molecules came into contact with various digestive enzymes in the digestive system and act as an inhibitor of α-amylase activity[14]. At the same time, the DBP molecules inevitably come into contact with the epithelial cells of the small intestine during the digestion process in the intestine. Then, the absorption of DBP was investigated through the transepithelial transport experiment using the Caco-2 cell monolayer. Before the cell transport test, the toxicity of DBP to Caco-2 cells was evaluated (Fig. 1A). As expected, the DBP was non-toxic to Caco-2 cells at concentrations between 0.25 and 1.5 mg/mL, which was not significantly different from that of the control ($P > 0.05$). The cell viability rate decreased as the DBP concentration increased above 1.5 mg/mL. The viability rate dropped to 77.25% at 2.5 mg/mL, confirming the cell proliferation inhibition effect caused by the higher DBP concentration. The above result proved the non-toxic nature of DBP to Caco-2 cells at a concentration lower than 0.5 mg/mL. Therefore, the DBP with appropriate concentration could be used safely in the following experiments.

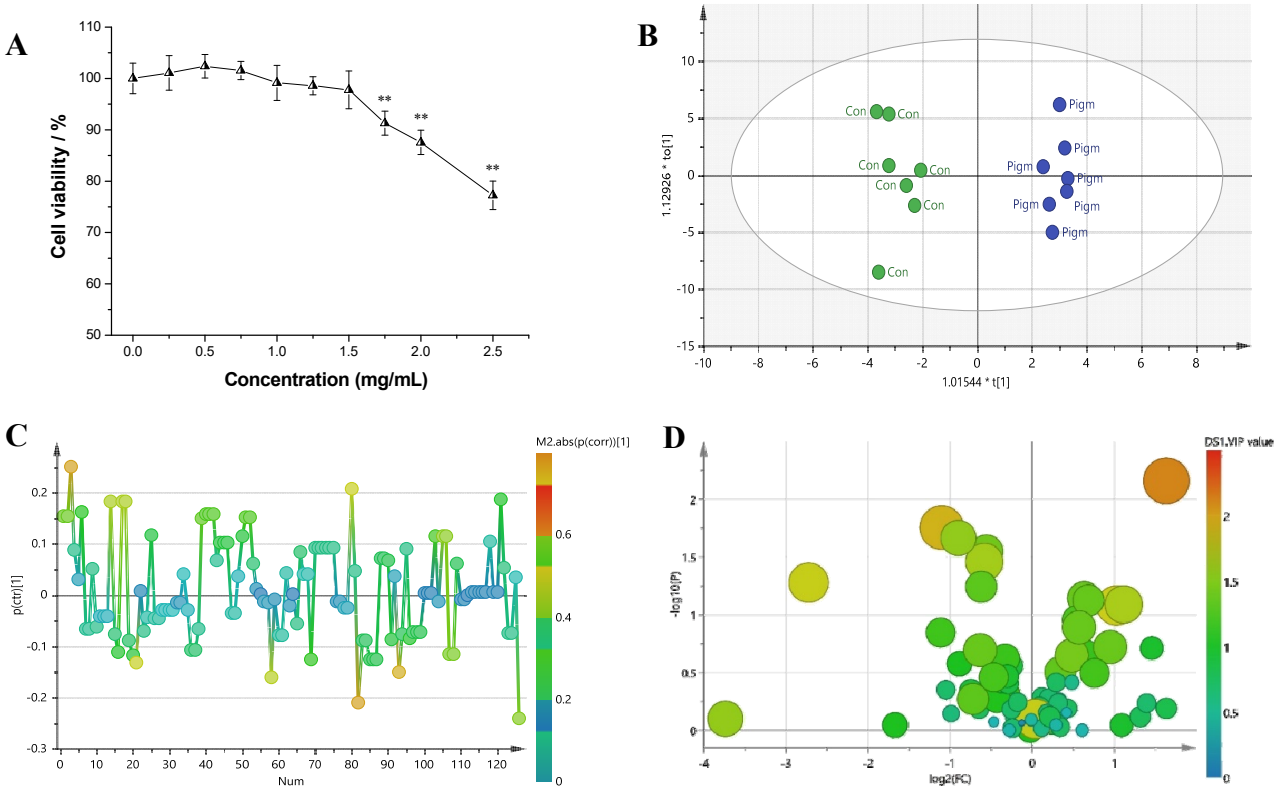

Fig. 1 (A) Viability in Caco-2 cells by DBP at different concentrations. Values are expressed as means ± SD (n=3). The '**' denote significant differences at $P < 0.05$. (B) Non-targeted endo-metabolites profiling distribution of Caco-2 cell treated by DBPs according to the OPLS-DA score plots, R^2=0.975, Q^2=0.665. The S-line for the OPLS-DA model of endo-metabolome of Caco-2 cells treated by DBP for 24 hours (C). The differential metabolites with VIP > 1.0 in S-plot were marked with red. S-line visualized the p(ctr) loading colored according to the absolute value of the correlation loading p(corr). (D) The volcano plot for the OPLS-DA model of endo-metabolites of Caco-2 cells treated by DBP for 24 hours. The volcano plot visualized the endo-metabolites colored according to the VIP value of the OPLS-DA model.

3.2 Multivariate statistical analysis for the metabolite profiling of Caco-2 cell

The active substances in natural products scavenge free radicals directly and regulate cell redox balance and metabolite synthesis[27]. In this study, the potential effects of DBP on the Caco-2 cell endo-metabolome were investigated by the orthogonal partial least squares discriminant analysis (OPLS-DA) using the dataset of endo-metabolites in Caco-2 cell. OPLS-DA is an extension of PLS-DA, which is based on splitting the variations of the variables into two components. The variation separation in OPLS-DA facilitates the interpretation of the model and the identification of the important variables, which was employed to divide the different cell group samples[28]. The Caco-2 cell intracellular metabolites were detected and processed by peak area normalization and then scaled by Pareto algorithm for OPLS-DA. The OPLS-DA model overview plot summarized the first two components in the endo-metabolome of the Caco-2 cell, as described in Fig. 1B. The high cumulative R^2 values (0.975) and Q^2 values (0.665) demonstrated the validity of the OPLS-DA model for endo-metabolome of Caco-2 cells treated by the DBP. The OPLS-DA analysis of UPLC-QToF-MS metabolic profiles of Caco-2 cells showed significantly separated clusters between the samples of the control group (Con) and DBP treated group (Pigm) in the OPLS-DA score plot, as shown in Fig. 1B. Both samples in the score plots were within the 95% Hotelling T2 ellipse. The OPLS-DA model scaled by Pareto algorithm is usually visualized by scaling of the OPLS coefficients. The fine structures of the original MS peaks of metabolites were maintained, and these two plot types were usually used in the discriminatory metabolite identification in Fig. 1B. Fig. 1C described the total of 126 metabolites as the S-line pattern: the positive *y*-axis illustrated an upregulated trend in DBP treated group compared with the control, and the negative *y*-axis showed a downregulated trend. Fig. 1C showed 70 upregulated metabolites and 56 down-regulated metabolites. Furthermore, the volcano plot of the total 126 metabolites was presented with $\log_2$ (fold change) as the *x*-axis and $-\log_{10}$ (*P* value) as the *y*-axis to visualize the changes in up- and down-regulation of metabolites in Caco-2 cells between the control and DBP treated groups (Fig. 1D). Based on the VIP value, the 28 differential metabolites with VIP > 1.0 were all screened for further pathway analysis according to VIP value > 1, the fold change value (FC < 0.67 and FC > 1.5), and *P* value<0.05 of the total metabolites.

3.3 Discriminatory metabolites screening and metabolic pathway analysis of Caco-2 cell

Fig. 2A exhibited the relative concentrations of screened endo-metabolites in each Caco-2 sample with heat maps generated by hierarchical Pearson clustering. The 28 metabolites were selected from the Caco-2 cell endo-metabolome by *p*-value, VIP value, and fold change value. Color scales range from bright yellow to deep orange, which indicated the up-regulation or down-regulation of the metabolites in DBP treated groups compared with control groups. The selected 28 endo-metabolites were displayed in the heatmap, which contained suberic acid (**1**), 4-hydroxycyclohexylcarboxylic acid (**2**), 3-phenoxypropionic acid (**3**), desamino tyrosine (**4**), L-3-phenyllactic acid (**5**), 3-methoxybenzenepropanoic acid (**6**), 16b-hydroxyestradiol (**7**), estriol (**8**), 3-methyladipic acid (**9**), pimelic acid (**10**), senecioic acid (**11**), 3,4-dihydroxymandelic acid (1**2**), sucrose (**13**), guanosine (**14**), 2-piperidinone (**15**), L-proline (**16**), 5-aminopentanoic acid (**17**), L-valine (**18**), N-methyl-a-aminoisobutyric acid (**19**), uracil (**20**), azelaic acid (**21**), D-arginine (**22**), L-arginine (**23**), nicotinic acid (**24**), picolinic acid (**25**), DL-2-aminooctanoic acid (**26**),

1-methylguanine (**27**), and 7-methylguanine (**28**). The heat map in Fig. 2A revealed the average levels between the control and DBP treated groups of these 28 differential metabolites after 24 h. It can be seen that the metabolites (**1~13**) showed upregulation in the DBP treated group, and the metabolites (**14~28**) showed a decreasing trend.

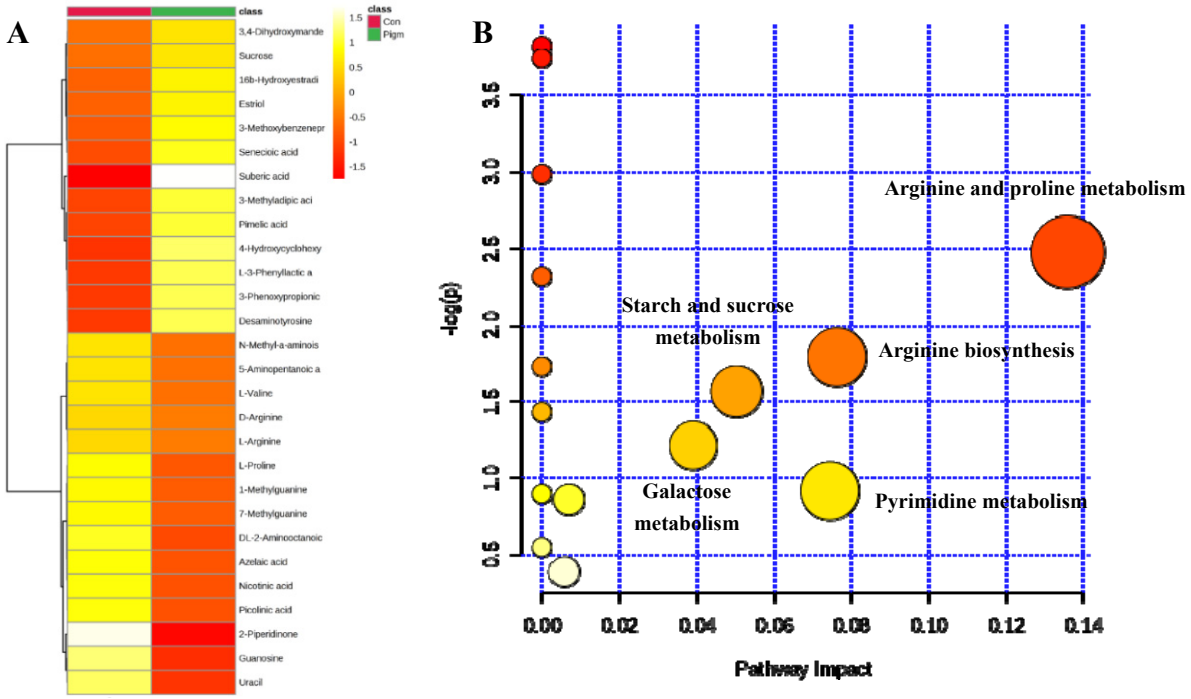

Fig. 2 (A) Heatmaps generated by Hierarchical Pearson clustering for the average level of differential endo-metabolites in Caco-2 cells. Color scales range from bright yellow to orange, which corresponds to the up-regulation or down-regulation of the metabolites. Con is the control group with red block, and Pigm is the DBP treated group with green block. (B) The pathway analysis of the identified metabolites in Caco-2 cells affected by DBP. The *x*-axis represents the pathway impact, and the *y*-axis represents the pathway enrichment. Larger sizes and darker colors represent higher pathway enrichment and higher pathway impact values.

Based on the web-based Metaboanalyst 5.0 pathway analysis, the integrating enrichment and pathway topology analysis was used to map the metabolic pathway of Caco-2 cells by the selected potential biomarkers[29]. According to the above results compared with the control and DBP treated group, metabolomics of Caco-2 cells detected significant changes in multiple small molecule metabolites, which played a critical role in cellular physiology. The intracellular metabolites of Caco-2 cells provide a more accurate pattern of the metabolic behavior in the cell. As shown in Fig. 2B, based on the metabolite matching of the KEGG metabolic pathway database, the metabolite enrichment results of the Caco-2 cell revealed that the arginine and proline metabolism, arginine biosynthesis, pyrimidine metabolism, starch and sucrose metabolism, and galactose metabolism were the main metabolic pathways affected by the DBP treatment. The impact values of all pathways were calculated using pathway topology analysis (Table 1), and the impact values for their metabolic pathways were 0.135 66, 0.076 14, 0.074 3, 0.050 23, and 0.038 88, respectively. In this MetaboAnalyst 5.0 pathway enrichment analysis, pathways with impact values > 0.1 meant the significantly affected metabolic pathways. Whereas, these enrichment analysis can only represent partial metabolic pathway results, and a single metabolic pathway distribution cannot comprehensively represent the changes in the whole pathway system and the correlation between these pathways. Therefore,

an integrated analysis of metabolic pathways was used to dissect the effects of DBP on metabolic pathways in the Caco-2 cell metabolome.

Table 1 Detailed results from the pathway analysis associated with the discriminatory metabolites.

	Pathway name	Hits	*P* value	-log(p)	Impact value
1	Arginine and proline metabolism	2/38	0.084 299	2.473 4	0.135 66
2	Arginine biosynthesis	1/14	0.166 89	1.790 4	0.076 14
3	Pyrimidine metabolism	1/39	0.401 22	0.913 25	0.074 3
4	Starch and sucrose metabolism	1/18	0.209 48	1.563 1	0.050 23
5	Galactose metabolism	1/27	0.297 88	1.211 1	0.038 88
6	Tyrosine metabolism	1/42	0.424 7	0.856 38	0.006 74
7	Steroid hormone biosynthesis	1/85	0.678 63	0.387 68	0.005 58
8	Aminoacyl-tRNA biosynthesis	1/48	0.0219 46	3.819 2	0
9	Pantothenate and CoA biosynthesis	1/19	0.023 723	3.741 3	0
10	D-Arginine and D-ornithine metabolism	1/4	0.050 671	2.982 4	0
11	Valine, leucine, and isoleucine biosynthesis	1/8	0.098 896	2.313 7	0
12	Nicotinate and nicotinamide metabolism	1/15	0.177 74	1.727 4	0
13	beta-Alanine metabolism	1/21	0.240 06	1.426 9	0
14	Valine, leucine and isoleucine degradation	1/40	0.409 14	0.893 69	0
15	Purine metabolism	1/65	0.577 77	0.548 57	0

Overall, the two metabolism pathways, metabolism of amino acids and glycometabolism, were the dominant types in the cellular physiology of mammals. Amino acids play important roles in many metabolic pathways as primary substrates and regulators[30]. In this study, arginine and proline metabolism and arginine biosynthesis were affected, including arginine (VIP=1.3487, Fold change value=1.638 6) and proline (VIP=1.63565, Fold change value=1.500 4), the expression of which was downregulated in the DBP treated groups. As the primary substrates for metabolic substrates, the amino acid is linked to amino acid catabolism and biosynthesis in the metabolic pathway. The KEGG database showed that arginine was involved in 38 physiological reactions, 20 pathways, and 27 enzymes (Table S3). The proline was involved in 17 physiological reactions, 14 pathways, and 16 enzymes (Table S4). Some researches had reported that the L-arginine and L-proline can enhance the proliferation of intestinal cells and prevent endotoxin-induced cell death[31-32]. The L-arginine was observed to ameliorate LPS-induced intestinal inflammation by inhibiting TLR4/NF-κB and MAPK pathways in *in vivo* and *in vitro* models[33]. But, according to the toxicity analysis of DBP-treated Caco-2 cells in this study, a concentration of 0.5 mg/mL did not cause growth inhibition or inflammatory response (Fig. S2), indicating that the physiological functions of Caco-2 cells could still work properly under these conditions.

The starch and sucrose metabolism and galactose metabolism were also affected, while the impact values were not significant. The sucrose, fructose, and rhamnose showed up-regulation in the DBP treated group, and the α-lactose, cellobiose, isomaltose, lactulose, melibiose, trehalose, and turanose showed down-regulation. Only sucrose showed a significant difference between the control and DBP treated groups (VIP value = 1.046 89, Fold change value = 3.173 5). Sucrose was involved in 24 reactions, 8 pathways, and 23 enzymes (Table S5). However, under the upregulation of sucrose, the Caco-2 cells could still keep their normal physiological functions through the compensation of other metabolism pathways[34].

3.4 Transepithelial absorption of dark blue pigment through Caco-2 cell monolayers

The influence of DBP samples with different concentrations on the transport across Caco-2 cell monolayer is shown in Fig. 3A. The absorption rate from the apical side to the basolateral side linearly increased as the DBP concentration increased from 0.25 mg/mL to 1.0 mg/mL (Fig. 3A). At the concentration of 0.25 mg/mL, the absorptive flux increased slowly with time, and a phenomenon of transmembrane transport was detected after the DBP contacted the cell monolayer for 8 h. As the DBP concentration gradually increased, the absorption rate increased along with time, presenting the growth curve with a rapid increase and then a gradual flattening. During the first 4 h of contact with the Caco-2 cell monolayer (Fig. 3B), the absorption efficiency increased linearly, and the cumulative absorption rates were 13.14%, 19.71%, and 40.30%, with 0.5, 0.75, and 1.0 mg/mL of DBP after 4 h of transport, and gradually saturated after 8 h. These results indicated that the absorption of DBP was dose-dependent, suggesting that the absorption process was a passive transport based on diffusion and migration.

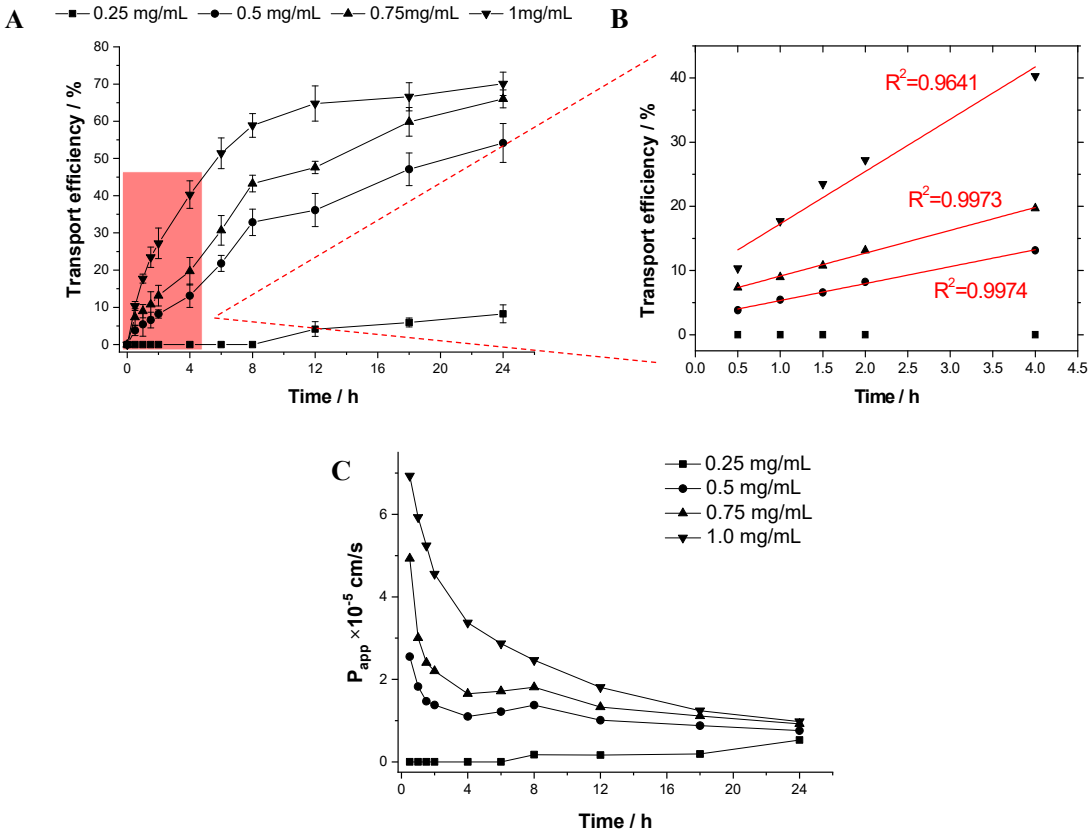

Fig. 3 (A) Effects of DBP on transport efficiency across Caco-2 cells monolayer. (B) Effects of DBP on apparent permeability coefficient (P_{app}) across Caco-2 cells monolayer (AP to BL direction) at different concentrations. (C) Effects of DBP on transport efficiency across Caco-2 cells monolayer before 240 min.

Fig. 3C showed the apparent permeability coefficients (P_{app}) of DBP. In the concentrations examined, $P_{app\ (AP\ to\ BL)}$ values were higher than 10^{-6} cm/s at all concentrations except for 0.25 mg/mL concentration. This indicated that the small intestine could absorb the DBP molecules since the P_{app} values below 10^{-6} cm/s demonstrated the poor cell permeability and absorption[35]. The $P_{app\ (AP\ to\ BL)}$ values increased with increasing the DBP concentration, indicating that the absorption efficiency of DBP exposed at higher concentrations was relatively high through the cell monolayer from the apical side. The $P_{app\ (AP\ to\ BL)}$ values during the 240 min of

transportation were (1.10 ± 0.19)×10^{-5} cm/s, (1.65 ± 0.21)×10^{-5} cm/s, and (3.37 ± 0.38)×10^{-5} cm/s for DBP concentrations of 0.5, 0.75, and 1.0 mg/mL, respectively. Considering the other transport modes, such as active efflux, the P_{app} of the BL to AP direction during 4 h of DBP transportation experiment was also studied on the Caco-2 monolayer (Table 2).

Table 2 Effect of concentration on apparent permeability coefficients (P_{app}) and R of DBP across Caco-2 cell monolayers.

	$P_{app\ (AP\ to\ BL)}$ ×10^{-5} cm/s	$P_{app\ (BL\ to\ AP)}$ ×10^{-5} cm/s	R
0.25 mg/mL	ND	ND	—
0.5 mg/mL	1.10 ± 0.19[a]	0.67 ± 0.10[a]	1.63
0.75 mg/mL	1.65 ± 0.21[b]	0.97 ± 0.14[b]	1.69
1.0 mg/mL	3.37 ± 0.38[c]	1.81 ± 0.32[c]	1.86

Data are means ± SD (n = 3). R is the ratio of $P_{app\ (AP\ to\ BL)}$ to $P_{app\ (BL\ to\ AP)}$. ND: not detected.

The DBP can be detected in both transport directions during the incubation, and the transported amount of DBP also increased with the higher DBP concentration. The P_{app} of DBP from the BL to AP side was calculated and summarized in Table 2. As shown, it can be seen that the P_{app} of DBP from the BL to AP side during 4 h of the transportation was lower than that from the AP to BL side at each DBP concentration. Also, the values of $P_{app\ (BL\ to\ AP)}$ of DBP at 0.5, 0.75, and 1.0 mg/mL were respectively 0.67×10^{-5} ± 0.10×10^{-5}, 0.97×10^{-5} ± 0.14×10^{-5}, and 1.81×10^{-5} ± 0.32×10^{-5} cm/s, which were all higher than 10^{-6} cm/s, indicating the higher cell permeability and absorption of DBP from the BL to AP direction on the Caco-2 monolayer[36]. Furthermore, compared with the P_{app} of the AP to BL, the ratio (R) of $P_{app\ (AP\ to\ BL)}$ to $P_{app\ (BL\ to\ AP)}$ at the concentrations of 0.5, 0.75, and 1.0 mg/mL were 1.63, 1.69, and 1.81, respectively, demonstrating that an active transport existed during the transportation of DBP in Caco-2 monolayer[37].

3.5 Changes in expression levels of potential transporters of dark blue pigment in Caco-2 cell

According to the absorption mode of DBP obtained above, the DBP molecules with good hydrophilicity can be absorbed via the combination of passive and active transport by the intestinal epithelial Caco-2 cells, but the potential transportors are still unclear. For the active transport of nutrients, their transporters contain the hexose transporters, and the ATP binding cassette transporters (ABC)[38]. Hexose transporters are located in the epithelial cells, consisting of sodium-dependent glucose cotransporters (SGLT1) and glucose/fructose transporters (GLUT2 and GLUT5). Previous studies indicated that both the transporters of SGLT and GLUT played an important role in the absorption of anthocyanin[21]. Since DBP (the iridoid-derived compounds) owned the same chemical structure with anthocyanin, we confirmed that the DBP could be transported from the basolateral side to the apical side in the Caco-2 cell monolayer, and the exposure of DBP at the concentration of 0.5 mg/mL increased the relative mRNA expression of GLUT2 and GLUT5 by 58% and 65%, respectively (Figs. 4A, B).

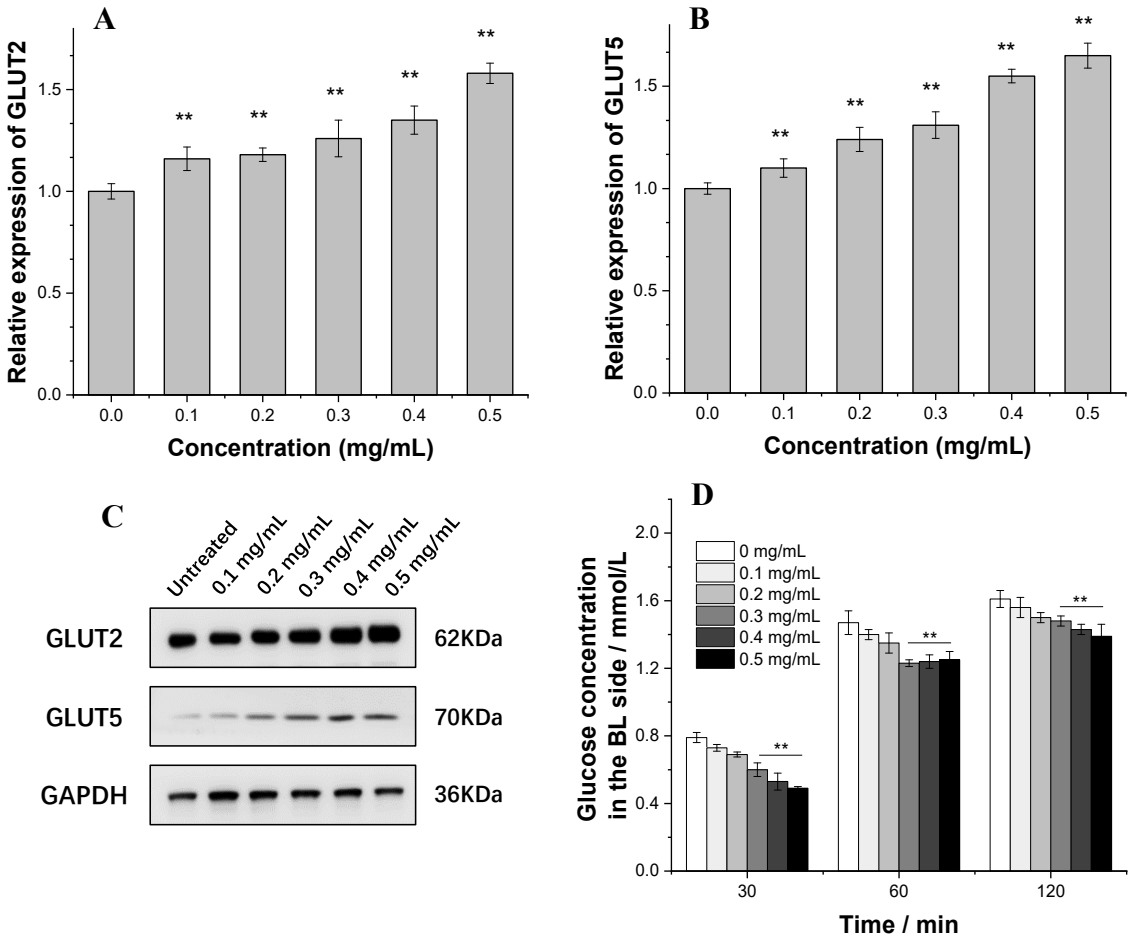

Fig. 4 Effect of DBP on the relative mRNA and protein expressions of potential transporters (A: GLUT2, B: GLUT5) in Caco-2 cells. (C) Protein expression of GLUT2 and GLUT5 after 12 h treatment. (D) Effect of DBP on glucose transport in Caco-2 cells. Results are presented as means ± SD, ** compared with the control group ($P < 0.05$).

Furthermore, the DBP treatment also significantly enhanced the protein expression of GLUT2 and GLUT5 (Fig. 4C). This indicated that the DBP could be absorbed mainly through the GLUT2 and GLUT5, which is consistent with the transportation of some anthocyanins[20]. Due to the role of the glucose uptake transporters (GLUT2 and GLUT5), these active compounds showed inhibitory effects on glucose uptake and transport via the steric hindrance or competitive manners during their transportation through the intestinal epithelial cells[39]. Furtherly, to verify the interference of DBP on the glucose transport of Caco-2 cells, the results in Fig. 4D showed a significant difference among control and DBP treatments. Owing to the treatment with different concentrations of DBP in 30 min, the glucose transport from AP to BL side was decreased significantly with the increasing DBP contents. The glucose transport amounts with 0.5 mg/mL of DBP were significantly lower than the control by the reduction of 38.0%. Additionally, DBP caused the inhibition lasting for about 120 min in glucose transport. It preliminarily implied that DBP had the pronounced inhibitory effects on glucose transportation mediated by GLUTs.

ABC transporters located in the intestinal enterocytes tend to facilitate the transportation of bioactive ingredients with small molecular weight, such as multi-drug resistance proteins (MRPs, MDR1/P-gp). The Caco-2 cells exposed to DBP at the concentration of 0.5 mg/mL significantly reduced the relative mRNA

expression of MDR1 and MRP2, which down-regulated the mRNA expression by 25% and 31%, respectively (Figs. S3A, B). Moreover, on the basis of the obtained results of increased amount of DBP transportation and GLUTs protein expression, the protein expression of MDR1 and MRP2 in Caco-2 cells was also restrained under DBP treatment compared to the untreated group (Fig. S3C). This indicated that the transporters of MDR1 and MRP2 may not be involved in transportation the DBP molecules. Nevertheless, the molecular size and structure of active compounds determined their transporters during the absorption through the intestinal epithelial cells[40]. Lewandowska et al reported that the phase II digested metabolites with small molecular size, such as protocatechuic acid, phenylpropionic acid, and dihydroxybenzoic acid, were inclined to be absorbed through the transporters of MDR1 and MRP2 via active transport[41].

3.6 Effects of dark blue pigment on mRNA expression levels of tight-junction proteins in Caco-2 cell

As the first defense against the environment in the intestinal lumen, the physical barrier formed by the epithelium cells and their connections plays an important role in the barrier structure of the intestinal tract. According to the effect of DBP on the arginine and proline metabolism above, arginine and proline tended to promote the development and proliferation of intestinal epithelial cells and repair after injury[31], while the arginine and proline both decreased during the DBP transportation (section 3.3). Therefore, this study assessed the potential effect of DBP on the intestinal barrier by measuring the mRNA expression of the intestinal tight junctions (TJs). TJs are the most crucial intercellular connections existing on the intestinal epithelial cell surface, which are a series of multiple transmembrane proteins and molecules, such as occludin, claudins, and zonula occludens (ZOs)[42-43].

As shown in Fig. 5, the DBP influenced the TJs' mRNA expression in the normal Caco-2 cells ($P < 0.05$). For occludin (Fig. 5A), the increase of mRNA relative expression of occluding was observed in Caco-2 cells with the increase of DBP concentration. The mRNA relative expression of claudin-1 was not affected by the exposure to DBP (Fig. 5B). For ZO-1 (Fig. 5C), the mRNA relative expression significantly decreased compared to the group treated without DBP ($P < 0.05$). Usually, the diet ingredients, disease, or oxidative stress in intestine tract can affect the barrier function of the intestine wall, which is accompanied by the important phenomenon of inflammation[16]. Therefore, the inflammation mode of oxidative-damaged Caco-2 cell *in vitro* was built to simulate dysfunction of the intestinal epithelial barrier along with the disruption of the mRNA expression of TJs. The mRNA relative expression of occludin, claudins, and ZO-1 significantly decreased in the oxidative-damaged Caco-2 cell compared with the normal Caco-2 cell (Figs. 5D-F). Noticeably, these reductions of TJs' mRNA expression in the oxidative-damaged model group were reversed by DBP administration ($P < 0.05$). The mRNA expression of occludin, claudins, and ZO-1 increased by the increasing dose of DBP. The relative expressions of occluding and claudins in Caco-2 cells treated by the 0.5 mg/mL of DBP were at the same expression level as the control group ($P > 0.05$) (Fig. 5D&E). These results indicated that the DBP owns recovery capability against oxidative-induced disruption of tight junctions in the intestine epithelial cells. Our previous studies proposed that the key active compounds in the DBP were the derivates of iridoid glycosides which owned the same protective effects on the intestinal epithelial cells as our

finding[12-13]. Liu & Wang[44] found that the protective effect on experimental colitis was observed through inhibition of epithelial cell apoptosis possessed and blockade of NF-κB signal pathway by iridoid glycoside treatment (the main component was syringopicroside). The other two iridoid glycosides, morroniside and loganin, also possessed protective effect on the inflammatory cells and acute colitis via increasing the expression of TJs and reducing the pro-inflammatory cytokine production[45].

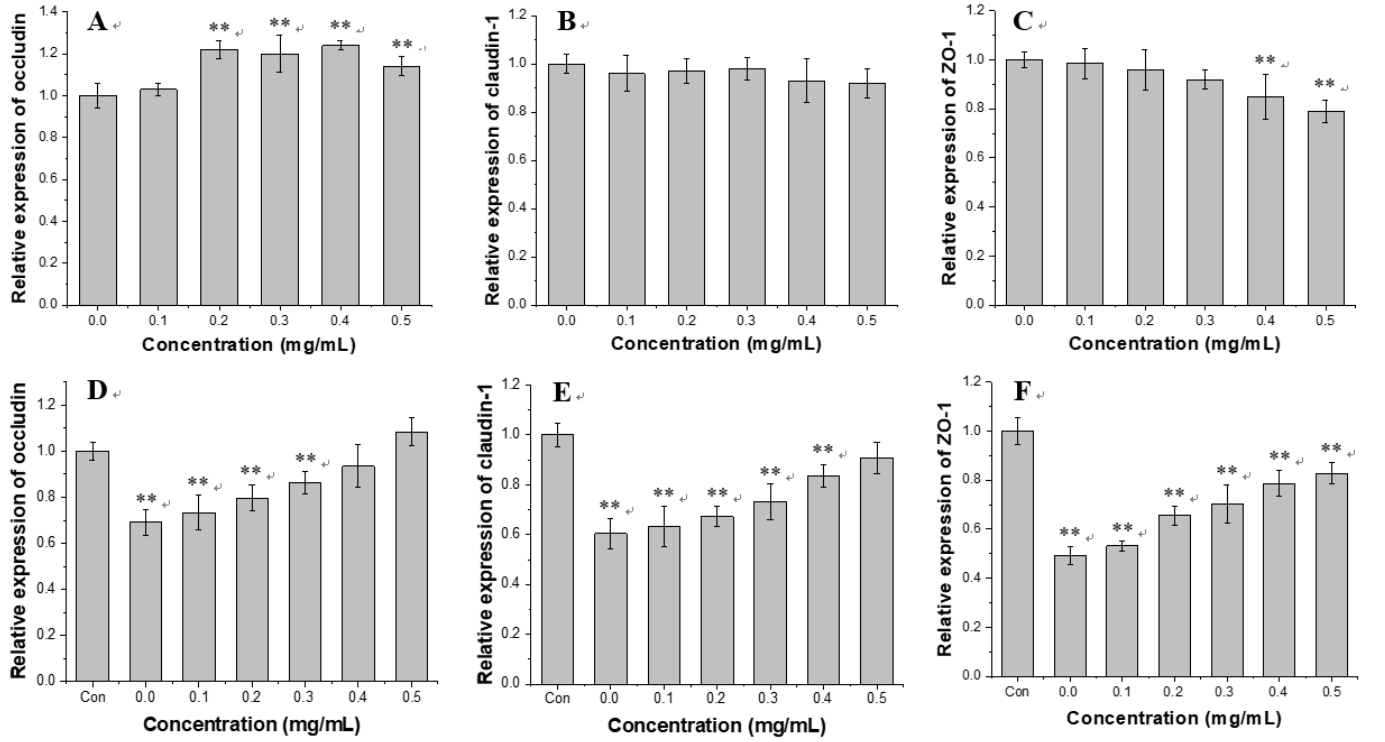

Fig 5 Effects of DBP on mRNA expression levels of three intestinal tight junction proteins (A-C) in the normal Caco-2 cell and the reverse of three intestinal tight junction proteins (D-F) in the oxidative-damaged Caco-2 cell at the exposure of DBP. Con group is the normal Caco-2 cell without being treated by H_2O_2. Results are presented as means ± SD, **compared with the Con group ($P < 0.05$).

4. Conclusions

This study investigated the transepithelial absorption of DBP in the Caco-2 cell monolayer model and the potential influences on Caco-2 cells. The DBP can be absorbed via the combination type of passive and active transport in the Caco-2 cell monolayer, and the absorptive pattern of DBP showed a dose-dependent manner when the concentration was more than 0.25 mg/mL. In the Caco-2 cell model, the mRNA and protein expression of glucose transporters (GLUT2 and GLUT5) increased, and the mRNA and protein expressions of multi-drug resistance proteins (MDR1 and MRP2) decreased. However, the decreased glucose transport amount suggested the potential inhibitory effects on glucose transport or uptake via the steric hindrance or competitive manners during DBP transportation. The only affected metabolism was arginine and proline metabolism in Caco-2 cell exposed by 0.5 mg/mL of DBP which did not cause disorder in the normal cell metabolism. In addition, the DBP showed protective effects on Caco-2 cells by upregulating the mRNA expressions of three tight junction proteins (occludin, claudin-1, and ZO-1) in the oxidative-damaged Caco-2

cell model. These findings provide a deep understanding of the mechanisms underlying the absorption process of DBP from VBTL.

Acknowledgements

This research was supported by the China Postdoctoral Science Foundation (2021M701462), the National Natural Science Foundation of China (32072254), Ministry of Science and Technology of China (2020YFC1606804), the Postdoctoral Research Funding Program of Jiangsu Province (2021K097A), the Fundamental Research Funds for the Central Universities (JUSRP121106), and the "Qing Lan Project" of Jiangsu Province.

Declaration of interests

The authors declare no competing financial interest.

References

[1] M.C. Fan, Y.H. Fan, Z.M. Rao, et al., Comparative investigation on metabolite changes in 'Wu mi' production by *Vaccinium bracteatum* Thunb. leaves based on multivariate data analysis using UPLC-QToF-MS, Food Chem. 286 (2019) 146-153. https://doi.org/10.1016/j.foodchem.2019.01.144.

[2] J. Zhang, C.J. Chu, X.L. Li, et al., Isolation and identification of antioxidant compounds in *Vaccinium bracteatum* Thunb. by UHPLC-Q-TOF LC/MS and their kidney damage protection, J. Funct. Foods 11 (2014) 62-70. https://doi.org/10.1016/j.jff.2014.09.005.

[3] C.J. Chu, X.L. Li, L. Xia, et al., Chemical constituents in leaves of *Vaccinium bracteatum* and their anti-complementary activity, Chinese Traditional and Herbal Drugs 45 (2014) 458-465. https://doi.org/10.7501/j.issn.0253-2670.2014.04.002.

[4] Y. M. Ren, C.Q. Ke, C. Tang, et al., Divaccinosides A-D, four rare iridoid glucosidic truxillate esters from the leaves of *Vaccinium bracteatum*, Tetrahedron Lett. 58 (2017) 2385-2388. https://doi.org/10.1016/j.tetlet.2017.05.013.

[5] J. Qu, X. Chen, C.S. Niu, Chemical constituents from *Vaccinium bracteatum*, China Journal of Chinese Materia Medica 39 (2014) 684–688. https://doi.org/ 10.4268/cjcmn20140426.

[6] L. Wang, X.T. Zhang, H.Y. Zhang, et al., Effect of *Vaccinium bracteatum* Thunb. leaves extract on blood glucose and plasma lipid levels in streptozotocin-induced diabetic mice, J. Ethnopharmacol. 130 (2010) 465-469. https://doi.org/10.1016/j.jep.2010.05.031.

[7] Y. Zheng, L. Chen, Y. Liu, et al., Evaluation of antimicrobial activity of water-soluble flavonoids extract from *Vaccinium bracteatum* Thunb. Leaves, Food Sci. Biotechnol. 28 (2019) 1853-1859. https://doi.org/10.1007/s10068-019-00634-4.

[8] S.H. Kwon, S.X. Ma, Y.H. Ko, et al., *Vaccinium bracteatum* Thunb. exerts anti-inflammatory activity by inhibiting NF-κB activation in BV-2 microglial cells, Biomol. Ther. 24 (2016) 543-551. https://doi.org/10.4062/biomolther.2015.205.

[9] D.R. Oh, Y. Kim, E.J. Choi, et al., Antidepressant-like effects of *Vaccinium bracteatum* in chronic restraint stress mice: Functional actions and mechanism explorations, American J. Chinese Med. 46 (2018) 357-387. https://doi.org/10.1142/S0192415X18500180.

[10] M.C. Fan, T.T. Li, Y. Li, et al., *Vaccinium bracteatum* Thunb. as a promising resource of bioactive compounds with health benefits: An updated review, Food Chem. 356 (2021) 129738. https://doi.org/10.1016/j.foodchem.2021.129738.

[11] M.C. Fan, Y.H. Fan, W.P. Huang, et al., Tentative characterization of precursor compounds and co-factors of pigment formation in production of 'Wu mi' from *Vaccinium bracteatum* Thunb. Leaves, Food Chem. 262 (2018) 199-205. https://doi.org/10.1016/j.foodchem.2018.04.101.

[12] K. Tsutsumiuchi, T. Toyoshima, F. Hasegawa, et al., Molecular structure of gardenia blue pigments by reaction of genipin with benzylamine and amino acids, J. Agric. Food Chem. 69 (2021) 3904-3911. https://doi.org/10.1021/acs.jafc.0c07948.

[13] W.J. Lian, M.C. Fan, T.T. Li, et al., A novel green synthesis approach for natural bluish-violet pigments derived from water extracts of *Vaccinium bracteatum* Thunb. Leaves, Ind. Crop. Prod. 142 (2019) 111862. https://doi.org/10.1016/j.indcrop.2019.111862.

[14] M.C. Fan, W.J. Lian, T.T. Li, et al., Characterization of promising natural blue pigment from *Vaccinium bracteatum* thunb. leaves: Insights of the stability and the inhibition of alpha-amylase, Food Chem. 32 (2020) 126962. https://doi.org/10.1016 /j.foodchem.2020.126962.

[15] D. Elshaer, J. Begun, The role of barrier function, autophagy, and cytokines in maintaining intestinal homeostasis, Semin. Cell Dev. Biol. 61 (2017) 51-59. https://doi.org/10.1016/j.semcdb.2016.08.018.

[16] J.J.V. Branca, M. Gulisano, C. Nicoletti, Intestinal epithelial barrier functions in ageing, Ageing Res. Rev. 54 (2019) 100938. https://doi.org/10.1016/j.arr.2019.100938.

[17] P. Artursson, K. Palm, K. Luthman, Caco-2 monolayers in experimental and theoretical predictions of drug transport, Adv. Drug Deliver. Rev. 64 (2012) 280-289. https://doi.org/10.1016/j.addr.2012.09.005.

[18] K. Schreck, M.F. Melzig, Intestinal saturated long-chain fatty acid, glucose and fructose transporters and their inhibition by natural plant extracts in caco-2 cells, Molecules 23 (2018) 2544. https://doi.org/10.3390/molecules23102544.

[19] E. Haughton, M.N. Clifford, P. Sharp, Monocarboxylate transporter expression is associated with the absorption of benzoic acid in human intestinal epithelial cells, J. Sci. Food Agr. 87 (2007) 239-244. https://doi.org/10.1002/jsfa.2703.

[20] A. Faria, D. Pestana, J. Azevedo, et al., Absorption of anthocyanins through intestinal epithelial cells - putative involvement of GLUT2, Mol. Nutr. Food Res. 53 (2009) 1430-1437. https://doi.org/10.1002/mnfr.200900007.

[21] T.B. Zou, D. Feng, G. Song, et al., The role of sodium-dependent glucose transporter 1 and glucose transporter 2 in the absorption of cyanidin-3-O-beta-glucoside in Caco-2 cells, Nutrients 6 (2014) 4165-4177. https://doi.org/10.3390/nu6104165.

[22] Q.J. Huang, Y.D. Zhu, L.S. Lv, et al., Translating in vitro acrolein-trapping capacities of tea polyphenol and soy genistein to *in vivo* situation is mediated by the bioavailability and biotransformation of individual polyphenols, Mol. Nutr. Food Res. 64 (2020) e1900274. https://doi.org/10.1002/mnfr.201900274.

[23] I. Fernandes, F. Nave, R. Gonçalves, et al., On the bioavailability of flavanols and anthocyanins: Flavanol-anthocyanin dimers, Food Chem. 135 (2012) 812-818. https://doi.org/10.1016/j.foodchem.2012.05.037.

[24] F. Han, H. Oliveira, N.F. Bras, et al., *In vitro* gastrointestinal absorption of red wine anthocyanins-impact of structural complexity and phase II metabolization, Food Chem. 317 (2020) 126398. https://doi.org/10.1016 /j.foodchem.2020.126398.

[25] X. Q. Xu, P. Y. Wang, B.G. Wang, et al., Glucose absorption regulation and mechanism of the compounds in *Lilium lancifolium* Thunb on Caco-2 cells, Food Chem. Toxicol. 149 (2021) 112010. https://doi.org/10.1016/j.fct.2021.112010.

[26] Y. Hou, L.H. Men, Z.F. Pi, et al., Fecal metabolomics of type 2 diabetic rats and treatment with Gardenia jasminoides ellis based on mass spectrometry technique, J. Agric. Food Chem. 66 (2018) 1591-1599. https://doi.org/10.1021/acs.jafc.7b06082.

[27] C.C. Chuang, M.K. McIntosh, Potential mechanisms by which polyphenol-rich grapes prevent obesity-mediated inflammation and metabolic diseases, Annu. Rev. Nutr. 31 (2011) 155-176. https://doi.org/10.1146/annurev-nutr-072610-145149.

[28] J. Ji, J.D. Sun, F.W. Pi, et al., GC-TOF/MS-based metabolomics approach to study the cellular immunotoxicity of deoxynivalenol on murine macrophage ANA-1 cells, Chem-biol. Interact. 256 (2016) 94-101. https://doi.org/10.1016/j.cbi.2016.06.017.

[29] J. Chong, O. Soufan, C. Li, et al., MetaboAnalyst 4.0: towards more transparent and integrative metabolomics analysis, Nucleic Acids Res. 46 (2018) W486-W494. https://doi.org/10.1093/nar/gky310.

[30] M.L. He, L. Li, H.H. Wang, et al., Effects of high-grain diet with buffering agent on the hepatic metabolism in lactating goats, Front. Physiol. 10 (2019) 661. https://doi.org/10.3389/fphys.2019.00661.

[31] J. Wang, B. Tan, J. Li, et al., Regulatory role of L-proline in fetal pig growth and intestinal epithelial cell proliferation, Anim. Nutr. 6 (2020) 438–446, https://doi.org/10.1016/j.aninu.2020.07.001.

[32] B. Tan, Y. Yin, X. Kong, et al., L-arginine stimulates proliferation and prevents endotoxin-induced death of intestinal cells, Amino Acids. 38 (4) (2010) 1227–1235, https://doi.org/10.1007/s00726-009- 0334-8.

[33] J. Lan, X. Dou, J. Li, et al., L-arginine ameliorates lipopolysaccharide-induced intestinal inflammation through inhibiting the TLR4/NF-κB and MAPK pathways and stimulating β-defensin expression *in vivo* and *in vitro*, J. Agric. Food Chem. 68 (2020) 2648–2663, https://doi.org/10.1021/ acs.jafc.9b07611.

[34] W.F. Cao, W.L. Cao, F. Shen, et al., A sustainable pH shift control strategy for efficient production of β-poly (L-malic acid) with $CaCO_3$ addition by Aureobasidium pullulans ipe-1, Appl. Microbiol. Biot. 104 (2020) 8691-8703. https://doi.org/10.1007/ s00253-020-10815-5.

[35] Y. Xu, Y. T. Li, J. H. Xie, et al., Bioavailability, absorption, and metabolism of pelargonidin-based anthocyanins using sprague−dawley rats and Caco-2 cell monolayers, J. Agric. Food Chem. 69 (2021) 7841-7850. https://doi.org/10.1021/ acs.jafc.1c00257.

[36] X.J. Tian, X.W. Yang, X.D. Yang, et al., Studies of intestinal permeability of 36 flavonoids using Caco-2 cell monolayer model, Int. J. Pharmaceut. 367 (2009) 58-67. https://doi.org/10.1016/j.ijpharm.2008.09.023.

[37] Y. Xu, Y.T. Li, J.H. Xie, et al., Bioavailability, absorption, and metabolism of pelargonidin-based anthocyanins using sprague–dawley rats and Caco-2 cell monolayers, J. Agric. Food Chem. 69 (2021) 7841-7850. https://doi.org/10.1021/ acs.jafc.1c00257.

[38] F. Alzaid, H.M. Cheung, V.R. Preedy, et al., Regulation of glucose transporter expression in human intestinal Caco-2 cells following exposure to an anthocyanin-rich berry extract, PLoS One 8 (2013) e78932. https://doi.org/10.1371/journal.pone.0078932.

[39] H. Zhang, Y.I. Hassan, J. Renaud, et al., Bioaccessibility, bioavailability, and anti-inflammatory effects of anthocyanins from purple root vegetables using mono- and co-culture cell models, Mol. Nutr. Food Res. 61 (2017) 1600928. https://doi.org/10.1002/mnfr.201600928.

[40] I. Fernandes, C. Marques, A. Evora, et al., Pharmacokinetics of table and port red wine anthocyanins: A crossover trial in healthy men, Food Funct. 8 (2017) 2030-2037. https://doi.org/10.1039/c7fo00329c.

[41] U. Lewandowska, K. Szewczyk, E. Hrabec, et al., Overview of metabolism and bioavailability enhancement of polyphenols, J. Agric. Food Sci. 61 (2013) 12183-12199. https://doi.org/10.1021/jf404439b.

[42] C.A.A. Hu, Y.Q. Hou, D. Yi, et al., Autophagy and tight junction proteins in the intestine and intestinal diseases, Anim. Nutr. 1 (2015) 123-127. https://doi.org/10.1016/ j.aninu.2015.08.014.

[43] S. Tsukita, H. Tanaka, A. Tamura, The claudins: From tight junctions to biological systems, Trends. Biochem. Sci. 44(2) (2019) 141-152. https://doi.org/10.1016/ j.tibs.2018.09.008.

[44] X. Liu, J.M. Wang, Iridoid glycosides fraction of folium syringae leaves modulates NF-κB signal pathway and intestinal epithelial cells apoptosis in experimental colitis, PLoS One 6 (2011) 1-12. https://doi.org/10.1371/journal.pone.0024740.

[45] J.H. Yuan, W.P. Cheng, G.Y. Zhang, et al., Protective effects of iridoid glycosides on acute colitis via inhibition of the inflammatory response mediated by the STAT3/NF-κB pathway, Int. Immunopharmacol. 81 (2020) 106240. https://doi.org/10.1016 /j.intimp.2020.106240.